# Current-interchange tearing modes: Conversion of interchange-type modes to tearing modes

L. J. Zheng[1] and M. Furukawa[2]

[1]*Institute for Fusion Studies, University of Texas at Austin, Austin, Texas 78712, USA*
[2]*Graduate School of Frontier Sciences, The University of Tokyo, Kashiwa, Chiba 277-8561, Japan*

It is shown that, in addition to usual neoclassical tearing modes, another type of nonclassical tearing mode exists in tokamaks: viz., current-interchange tearing modes (CITMs). CITMs are directly driven by unstable pressure-driven electromagnetic or electrostatic modes of the interchange type (e.g., interchange/ballooning modes, drift waves, etc.) due to the current gradient in tokamaks. Interchange-type modes exchange not only thermal and magnetic energies between flux tubes but also current. In a plasma with a current (or resistivity) gradient, such an interchange can create a current sheet at a mode resonance surface and result in the excitation of CITMs. Note that the interchange mode (i.e., Rayleigh–Taylor instability) is fundamental to tokamak physics. This new theory has an effect on both resistive magnetohydrodynamic stability and transport theories. Instabilities of the interchange type could be directly converted into CITMs, alternative to forming turbulent eddies through nonlinear coupling as in conventional transport theories. In particular, our CITM theory fills in the component in the transport theory of Rechester and Rosenbluth [Phys. Rev. Lett. **40**, 38 (1978)] for the origin of magnetic island structure in axisymmetric tokamaks. © *2010 American Institute of Physics*. [doi:10.1063/1.3425857]

## I. INTRODUCTION

Neoclassical tearing modes (NTMs)[1,2] are important for high-beta confinement of tokamak plasmas, where classical tearing modes are usually stable. In this paper we show that, there exists another type of nonclassical tearing mode in tokamaks. We refer our newly discovered non classical tearing mode as current-interchange tearing modes (CITMs), since they are directly driven by unstable electromagnetic and electrostatic modes of the interchange type (e.g., interchange/ballooning modes, drift waves, etc.) Interchange-type modes exchange not only thermal and magnetic energies between flux tubes but also current. In a plasma with resistivity (or current) gradient, such an interchange can create a current sheet at a mode resonance surface and result in the excitation of CITMs.

Since representing a new type of nonclassical tearing modes, CITMs can help to further clarify the NTM experiments.[3] In particular, our theory may explain why sometimes the resistive wall modes and NTMs are tied together in the experimental observation. The current CITM picture can also provide a natural explanation of the conversion from kink modes, for example, the $n=1$ internal kink modes, to tearing modes, where $n$ is the toroidal mode number. This may help to explain the tokamak plasma internal disruptions.[4,5]

CITMs are interesting not only because they represent a new type of nonclassical tearing mode but also because they may affect the development of the interchange type of modes, which are fundamental to tokamak physics. Instabilities of the interchange type have been widely used to model anomalous transport in tokamaks in terms of the formation of turbulent eddies through nonlinear coupling. Our new theory allows another route for the development. Interchange-type instabilities could be directly converted into CITMs, instead of developing into the pure interchange nonlinear state. The current theory is particularly relevant for clarifying the source of electron transport in tokamaks. In particular, our CITM theory fills in the component in the Rechester and Rosenbluth transport theory[6] for the origin of magnetic island structure in axisymmetric tokamaks. The electron energy transport observed experimentally is much larger than what one would expect from diffusive process due to Coulomb collisions. In Ref. 6, the broken magnetic surfaces due to formation of the magnetic island and stochastic field lines are used to explain the enhanced electron transport. However, how magnetic islands are formed in axisymmetric tokamak plasmas has not been given. The microtearing instabilities driven by electron temperature gradient are also proposed in this field for explaining the formation of the magnetic islands.[7] However, this type of modes are usually stable in conventional tokamaks except near the plasma edge.[7] Our current theory shows that the modes of interchange type can convert to tearing modes and result in the magnetic island structure. The mode types which can cause broken magnetic surfaces are broad based on our current theory. Secondary excitation of tearing modes by nonlinear pressure-driven mode turbulence had been reported in NIMROD code calculations,[8] in which the anomalous resistivity excited by the nonlinear pressure-driven modes was taken into consideration. In this paper we show, however, that the excitation of tearing modes by interchange-type modes can occur even in the linear stage, when the effect of the resistivity gradient is taken into account.

The effect of the resistivity gradient was first considered in the early 1960s, but only in relation to the rippling mode.[9] The resistivity gradient effect was addressed recently in
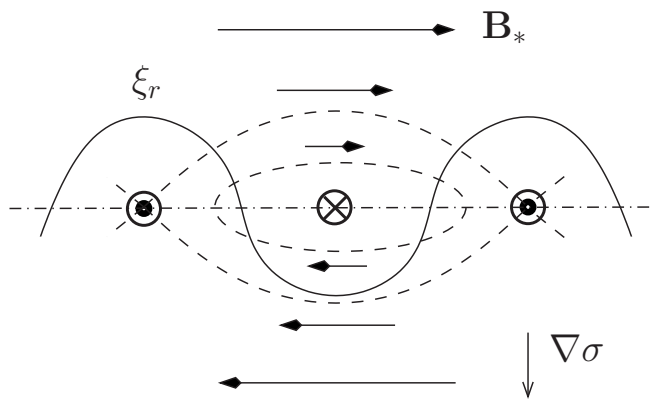
FIG. 1. The schematic picture for the formation of magnetic island at the rational surface due to the pressure-driven modes.

relation to tearing mode saturation,[10] but not for the CITMs that are reported for the first time in this paper.

This paper is arranged as follows. In Sec. II, the existence of CITMs is proved; in Sec. III, the physics implication of CITMs on anomalous transport and magnetohydrodynamic (MHD) phenomena is discussed; and in Sec. IV, summary is presented.

## II. EXISTENCE OF CURRENT INTERCHANGE TEARING MODES

In this section, the existence of CITMs is demonstrated from three aspects: the intuitive physics analysis, the linear analysis, and the nonlinear analysis. These analyses show that CITMs are crucial for tokamak physics, in that CITMs represent another developing route for pressure drive modes: converting to tearing type of modes. Therefore, they are essential for considering tokamak anomalous transport.

### A. Physics analysis

We first briefly explain the physical basis for the conversion of pressure-driven modes to CITMs, i.e., for the existence of CITMs. Figure 1 gives a schematic picture for this mode conversion process. We consider a rational surface (dot-dashed line). The minor radius points up, and therefore the gradient of the plasma electric conductivity $\nabla\sigma$ points down. Both the magnetic field and the Ohmic current at the rational surface are directed out of the plane of Fig. 1. The equilibrium magnetic field in the orthogonal direction with respect to the magnetic field on the rational surface, $\mathbf{B}_*$, is denoted by horizontal arrows. Boldface is used to denote vectors. $\mathbf{B}_*$ switches its direction across the rational surface. If the system is unstable to pressure-driven modes, a radial plasma displacement $\xi_r$ of the interchange type (solid curve) develops. In the conventional physical picture for the Rayleigh–Taylor instability, these perturbations develop when the total thermal and magnetic energy is reduced. Because the electric conductivity in tokamaks is generally inhomogeneous, the equilibrium current profile is not flat in the radial direction. Consequently, interchange-type perturbations carry not only plasma and magnetic energies but also current, by carrying along plasma temperature. This creates

alternating hills and holes of plasma current at the rational surface. Where plasma balloons out from the core, a current hill is created (denoted in Fig. 1 by circled dots). Instead, Where plasma shrinks to the core, a current hole is created, which is equivalent to a perturbed current being formed that is opposite to the equilibrium current at the rational surface. In Fig. 1, a current hole is denoted by a circled X. A current hill induces a counterclockwise magnetic field, whereas a current hole gives rise to a clockwise magnetic field. When these perturbed magnetic fields are added to the equilibrium magnetic field $\mathbf{B}_*$, the result is a magnetic island chain, denoted by the dashed curves in Fig. 1. This explains the mode conversion process from pressure-driven to current-driven tearing modes in tokamak plasmas.

### B. Linear analysis

In this subsection, we demonstrate the existence of CITMs in the linear theory framework. We consider high $n$ or radially localized modes, where $n$ is the toroidal mode number. The time ($t$) dependence is assumed to be $\exp\{\gamma t\}$, where $\gamma$ is the growth rate. The basic set of equations is derived from the equation of motion (or the so called vorticity equation), Ohm's law, and Maxwell's equations

$$\mathbf{B}\cdot\nabla\frac{\mathbf{B}\cdot\delta\mathbf{J}}{B^2} + 2\frac{\mathbf{B}\times\boldsymbol{\kappa}}{B^2}\cdot\nabla\delta p + \nabla\cdot\left(\frac{\mathbf{B}}{B^2}\times\rho_m\gamma^2\boldsymbol{\xi}\right) = 0,$$
$$(1)$$

$$\delta\mathbf{J} = \sigma(\delta\mathbf{E} + \gamma\boldsymbol{\xi}\times\mathbf{B}) + \delta\sigma\mathbf{E}, \qquad (2)$$

$$\delta p = -\boldsymbol{\xi}\cdot\nabla p, \qquad (3)$$

$$\delta\sigma = -\boldsymbol{\xi}\cdot\nabla\sigma, \qquad (4)$$

$$\delta\mathbf{J} = \nabla\times\delta\mathbf{B}, \qquad (5)$$

$$\gamma\delta\mathbf{B} = -\nabla\times\delta\mathbf{E}, \qquad (6)$$

where $\mathbf{B}$ and $\mathbf{E}$ denote, respectively, the magnetic and electric fields, $\mathbf{J}$ is the current density, $p$ represents the plasma pressure, $\rho_m$ denotes the mass density, $\boldsymbol{\xi}$ is the fluid displacement, $\boldsymbol{\kappa} = \mathbf{b}\cdot\nabla\mathbf{b}$ is the magnetic field line curvature, $\mathbf{b} = \mathbf{B}/B$, $\sigma$ is the electric conductivity, bold face is used to denote the vectors, and perturbed quantities are tagged with $\delta$. Here we have considered incompressible plasmas. Noting that the conductivity is a function of temperature and density, we have also introduced the convective perturbation for it in Eq. (4), as that for the plasma pressure in Eq. (3).[9]

We follow the standard approach to reduce the basic set of Eqs. (1)–(6).[11] The Hamada coordinates $(v, \theta, \zeta)$ are used, $v$ is the volume, $\theta$ is the generalized poloidal angle, and $\zeta$ represents the generalized toroidal angle. We also introduce the ballooning mode representation for perturbed quantities[12,13]

$$\delta\varphi_{m\pm k}(nq) = \delta\varphi(nq \mp k), \quad \text{for } k = 1, 2, \cdots,$$

$$(7)$$

$$\delta\varphi(x) = \int_{-\infty}^{\infty} d\theta \delta\varphi(\theta) \exp\{-inqsx\theta\},$$

where $m$ is poloidal mode number, $x = (v - v_s)/2v_s$, $s = 2v_s(dq/dv)/q$ is the magnetic shear, and $v_s$ represents the reference surface. With the stream functions introduced ($\boldsymbol{\xi}_\perp \propto \mathbf{b} \times \delta\varphi$ and $\delta\mathbf{B}_\perp \propto \mathbf{b} \times \nabla \delta\psi$), the following two coupled equations can be obtained from Eqs. (1)–(6):

$$\frac{\partial}{\partial\theta}\left(\frac{\dot{\chi}^3}{B^2}\mathbf{C}^2\delta\psi\right) + 2\dot{p}(\kappa_v + \kappa_\zeta\dot{q}\theta)\delta\varphi - \rho\gamma^2\frac{\dot{\chi}^2}{B^2}\mathbf{C}^2\delta\varphi = 0,$$

$$(8)$$

$$[1 + (n^2\eta/\gamma)\mathbf{C}^2]\delta\psi = \dot{\chi}\frac{d\delta\varphi}{d\theta} + i\frac{\Sigma'}{\gamma}\delta\varphi,$$

$$(9)$$

where $\mathbf{C}^2 = (\nabla\zeta - \dot{q}\theta\nabla v)^2$, $\Sigma' = (1/\dot{\chi})nqE_\phi(d\ln\sigma/dv)$, $E_\phi$ is toroidal equilibrium electric field, $\kappa_v$ and $\kappa_\zeta$ are covariant components of the curvature $\boldsymbol{\kappa}$, and dot denotes derivative with respect to $v$. Equations (8) and (9) can be combined to give the following equation:

$$\frac{\partial}{\partial\theta}\left[\frac{1}{B^2}\frac{\mathbf{C}^2}{1 + (n^2\eta/\gamma)\mathbf{C}^2}\left(\frac{\partial}{\partial\theta}\delta\varphi + i\frac{\Sigma'}{\gamma}\delta\varphi\right)\right]$$
$$+ \frac{2\dot{p}}{\dot{\chi}^4}(\kappa_v + \dot{q}\theta\kappa_\zeta)\delta\varphi - \rho\gamma^2\frac{1}{\dot{\chi}^2B^2}\mathbf{C}^2\delta\varphi = 0.$$

$$(10)$$

### 1. Conversion from resistive interchange modes to CITMs in the cylinder limit

To get an elucidating picture for the conversion from resistive interchange modes to CITMs, we first investigate the resistivity gradient effect on resistive interchange modes in the cylinder limit.[11,14] In this case, it is assumed that $(\eta/\gamma)\mathbf{C}^2 \gg 1$. With cylindrical symmetry, the geodesic curvature $\kappa_\zeta = 0$ vanishes and the equilibrium quantities become independent of $\theta$. Therefore, Eq. (10) reduces to

$$\frac{\partial^2\delta\varphi}{\partial\theta^2} + i\frac{\bar{\Sigma}'}{\gamma}\frac{\partial\delta\varphi}{\partial\theta} + (ns\sqrt{\gamma\eta}\Lambda - \gamma\eta n^2 s^2\theta^2)\delta\varphi = 0, \quad (11)$$

where $\Lambda = 2n\dot{p}\kappa_v|1/\dot{q}|\nabla v|\dot{\chi}^3|(\eta/\rho\gamma^3)^{1/2}$ and $\bar{\Sigma}' = \Sigma'|\dot{\chi}/n\dot{q}|\nabla v||(\eta/\rho\gamma^3)^{1/2}$. The second term in this equation is due to the resistivity gradient effect.

Equation (11) can be reduced to Kummer's equation[15]

$$z\frac{d^2\delta u}{dz^2} + \left(\frac{3}{2} - z\right)\frac{d\delta u}{dz} - \left(\frac{3}{4}\frac{\bar{\Sigma}'^2/\gamma^2 + 4ns\sqrt{\gamma\eta}\Lambda}{16ns\sqrt{\gamma\eta}}\right)\delta u = 0,$$

$$(12)$$

by the following two consecutive transforms:

$$\delta\varphi = \theta^{-1/2}e^{-i(1/2)(\bar{\Sigma}'/\gamma)\theta}\delta F,$$

$$\delta F = z^{3/4}e^{-(1/2)z}\delta u(z).$$

Here, $z = ns\sqrt{\gamma_N\eta}\theta$. Kummer's equation, Eq. (12), can be solved analytically. The eigenfunction is

$$\delta\varphi = (n^2s^2\gamma\eta)^{1/8}2^{-k}e^{-i(\bar{\Sigma}'/2\gamma)\theta - (1/2)ns\sqrt{\gamma\eta}\theta^2}H_k[(n^2s^2\gamma\eta)^{1/4}\theta],$$

$$(13)$$

with the eigenvalue determined by the following dispersion relation:

$$\frac{\bar{\Sigma}'^2/\gamma^2 + 4ns\sqrt{\gamma\eta}\Lambda}{4ns\sqrt{\gamma\eta}} = 2k + 1.$$

$$(14)$$

Here, $k = 0, 1, 2, \cdots$ and $H_k$ is the Hermite polynomial.

Without the resistivity gradient effect (i.e., $\bar{\Sigma}' = 0$), the dispersion relation in Eq. (14) reduces to the resistive interchange stability condition in Refs. 11 and 14: $\dot{p}\kappa_v < 0$, which is more stringent than the Suydam criterion.[16] The dispersion relation in Eq. (14) shows the resistivity gradient on the growth rate. For tokamaks, the loop voltage is a few volts and the equilibrium magnetic field is several tesla. Hence, the dimensionless parameter $\bar{\Sigma}'$ is of order of $10^{-5} - 10^{-4}$ as compared to the Alfvén frequency $\Omega_A$. Using this estimate, one can see that, for $\gamma/\Omega_A \sim 10^{-3}$, the $\bar{\Sigma}'$ effect on growth rate is not dramatical. However, the $\bar{\Sigma}'$ effect on the conversion from resistive interchange modes to CITMs is significant. This can be seen from the eigenfunction in Eq. (13). Without the resistivity gradient effect, the eigenfunction is symmetric with respect to $\theta$. Using Eq. (9), one can see that the perturbed radial magnetic field $\psi$ is odd in this case. Therefore, the perturbed radial magnetic field vanishes at the rational surface and no field line reconnection can occur. In the presence of the resistivity gradient effect (i.e., $\bar{\Sigma}' \neq 0$), the eigenfunction $\delta\varphi$ becomes complex and nonsymmetric and consequently an even (i.e., tearing mode parity) component of the perturbed radial magnetic field appears. This is due to the factor $\exp\{-i\bar{\Sigma}'\theta/(2\gamma)\}$ in the eigenfunction in Eq. (13). Because the resistive modes are localized in the configuration space, they extend broadly along the ballooning mode space. The coordinate $\theta$ can be a few tens to hundred. This makes this factor to be finite. This factor breaks the resistive interchange mode symmetry and gives rise to the tearing parity modes. As well-known, a nonvanishing radial magnetic field at the rational surface can cause the field line reconnection. This shows the conversion from resistive interchange modes to CITMs. This also shows that CITMs are different from the so-called rippling modes,[9] which also results from resistivity gradient.

### 2. Conversion from ballooning modes to CITMs

It is also interesting to see how the pressure driven modes are converted to CITMs in the toroidal geometry. We use the ballooning representation to account for the toroidal coupling. We consider the $s - \alpha$ equilibrium model.[13] In this equilibrium, the ballooning mode equation in Eq. (10) becomes
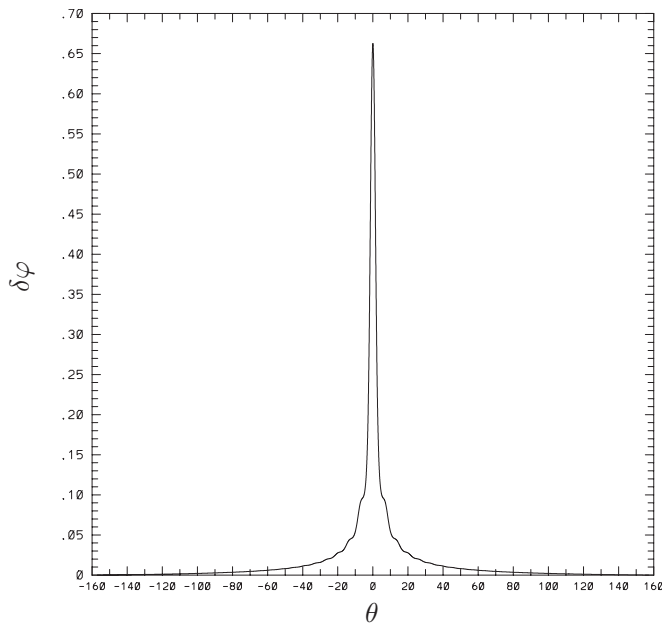
FIG. 2. Ideal MHD ballooning mode eigenfunction.



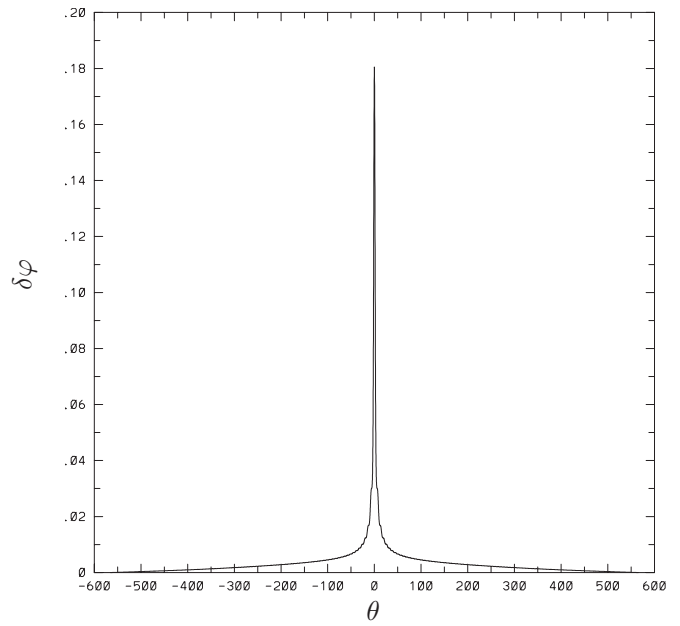FIG. 4. Resistive MHD ballooning mode eigenfunction.

$$\frac{\partial}{\partial \theta}\left[\frac{\bar{\mathbf{C}}^2}{1+(\eta^*/\gamma_N)\bar{\mathbf{C}}^2}\left(\frac{\partial}{\partial \theta}\Phi + i\frac{\Sigma'^*}{\gamma_N}\delta\varphi\right)\right]$$

$$+ \alpha\{\cos \theta + f(\theta)\sin \theta\}\delta\varphi - \gamma_N^2\bar{\mathbf{C}}^2\delta\varphi = 0, \qquad (15)$$

where $\eta^* = n^2\eta/(R^2\Omega_A)$, $\Sigma'^* = \bar{\Sigma}'/\Omega_A$, $\bar{\mathbf{C}}^2 = 1 + f^2(\theta)$, and $f(\theta) = s\theta - \alpha \sin \theta$.

We solve Eq. (15) numerically using Adaptive EiGen-function Independent Solution-1 Dimension (AEGIS-1D)code. AEGIS-1D code is a linear adaptive shooting code in the ballooning representation space, supplementary to the two dimensional (2D) AEGIS code[17] for high-n ballooning

calculation. The same numerical scheme as the 2D AEGIS is used in AEGIS-1D code. The general solution is decomposed by the independent solutions, the adaptive numerical shooting method is used to obtain the independent solutions, and multiple region matching technique is employed to find the eigenvalue and eigenfunction. This numerical scheme is particularly helpful for the computation of resistive modes, since they extend broadly along the field line. For $s-\alpha$ equilibrium, the code recovers the conventional $s-\alpha$ stability boundaries.[13,18] For $s=0.5$ case, it is found that the marginal stability $\alpha=0.386$. The eigenfunction $\delta\varphi$ for $\alpha=0.389$ is given in Fig. 2 with growth rate $\gamma_N=5.39\times 10^{-3}$. The per-
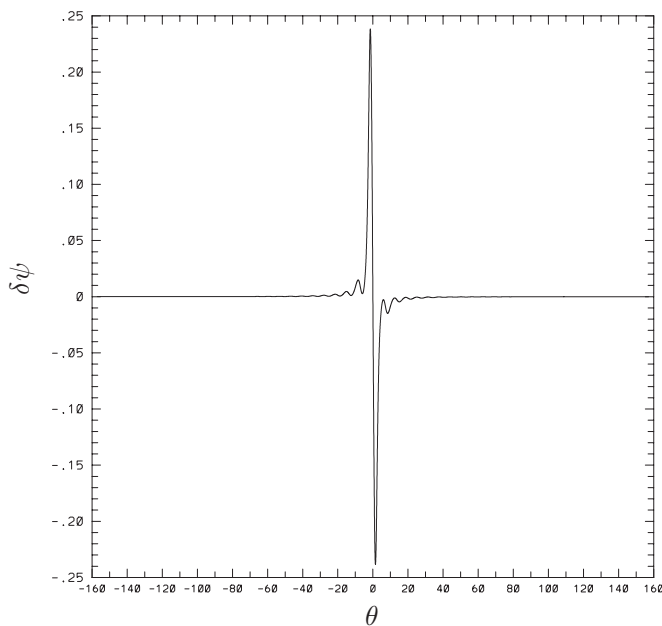


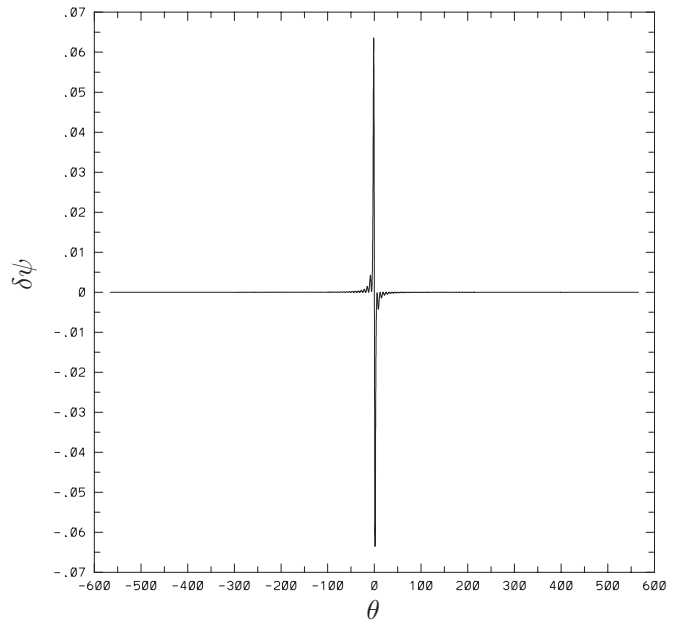FIG. 3. The perturbed radial magnetic field for ideal MHD ballooning mode.



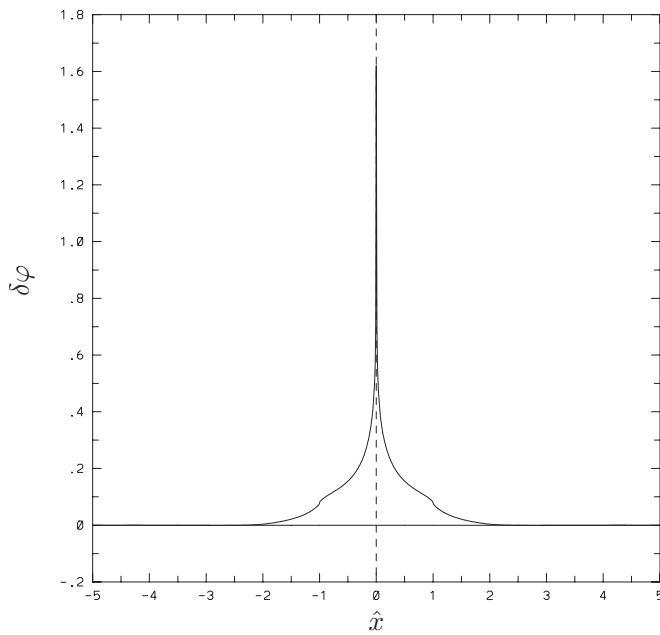FIG. 5. The perturbed radial magnetic field for resistive MHD ballooning mode.

FIG. 6. Resistive MHD ballooning mode eigenfunction in configuration space.



FIG. 8. Real and imaginary parts of the CITM eigenfunction.

turbed radial magnetic field $\delta\psi$ is also calculated and plotted in Fig. 3. From Fig. 3, one can see that $\delta\psi$ is odd. This is therefore a pure interchange-type of modes.

When small resistivity $\eta^*=10^{-6}$ is taken into account, while keeping $\Sigma'^*=0$, the unstable mode can be found in the stability regime for ideal MHD ballooning modes. For example, for the case with $s=0.5$ and $\alpha=0.38$, an unstable resistive ballooning modes with growth rate $\gamma_N=4.28\times10^{-3}$ can be obtained. The eigenfunction $\delta\varphi$ is given in Fig. 4 and the perturbed radial magnetic field $\delta\psi$ is plotted in Fig. 5. To see the mode behavior in the configuration space, we transform back the eigenfunction $\delta\varphi$ and the
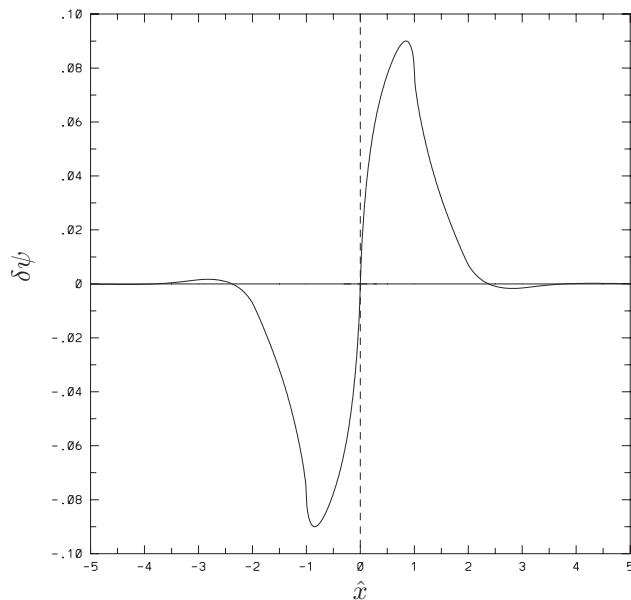


FIG. 7. The perturbed radial magnetic field for resistive MHD ballooning mode in configuration space.
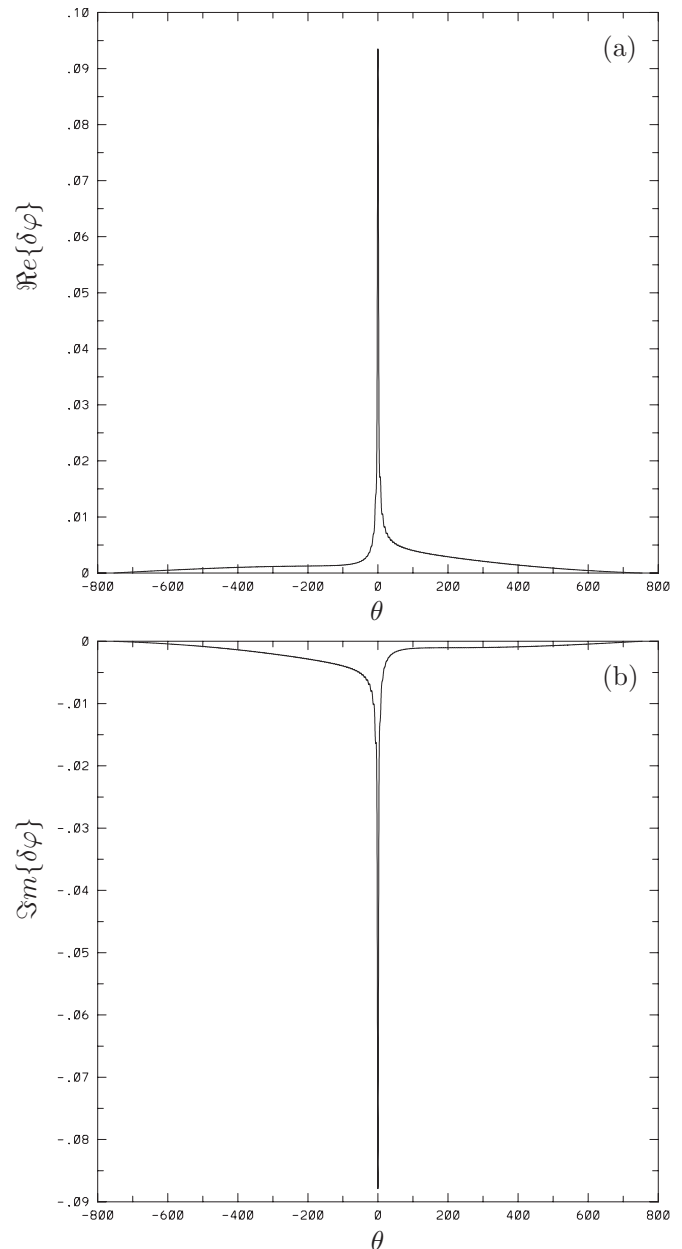
perturbed radial magnetic field $\delta\psi$ onto the configuration space, using Eq. (7). The results are plotted in Figs. 6 and 7. As one can expect, the resistive modes extend more broadly along the $\theta$ coordinate in the ballooning mode representation space, or more localized in the configuration space. In the current $s-\alpha$ coordinate, the so-called $\Delta'$ (the relative jump of the gradient of the perturbed radial magnetic field) is zero. Therefore, there are no tearing modes excited. This is clearly seen from the symmetry of the eigenfunction. This symmetry of resistive modes in $s-\alpha$ equilibrium can be seen from examining the ballooning mode equation in Eq. (15).

When the resistivity gradient is taken into account ($\Sigma'^*\neq0$), the symmetry of the ballooning equation, Eq. (15), is broken. We also consider the case with $s=0.5$, $\alpha=0.38$ and $\eta^*=10^{-6}$ as in the purely resistive ballooning mode case in Figs. 4–7. The ordering of $\Sigma'^*$ can be obtained from that of
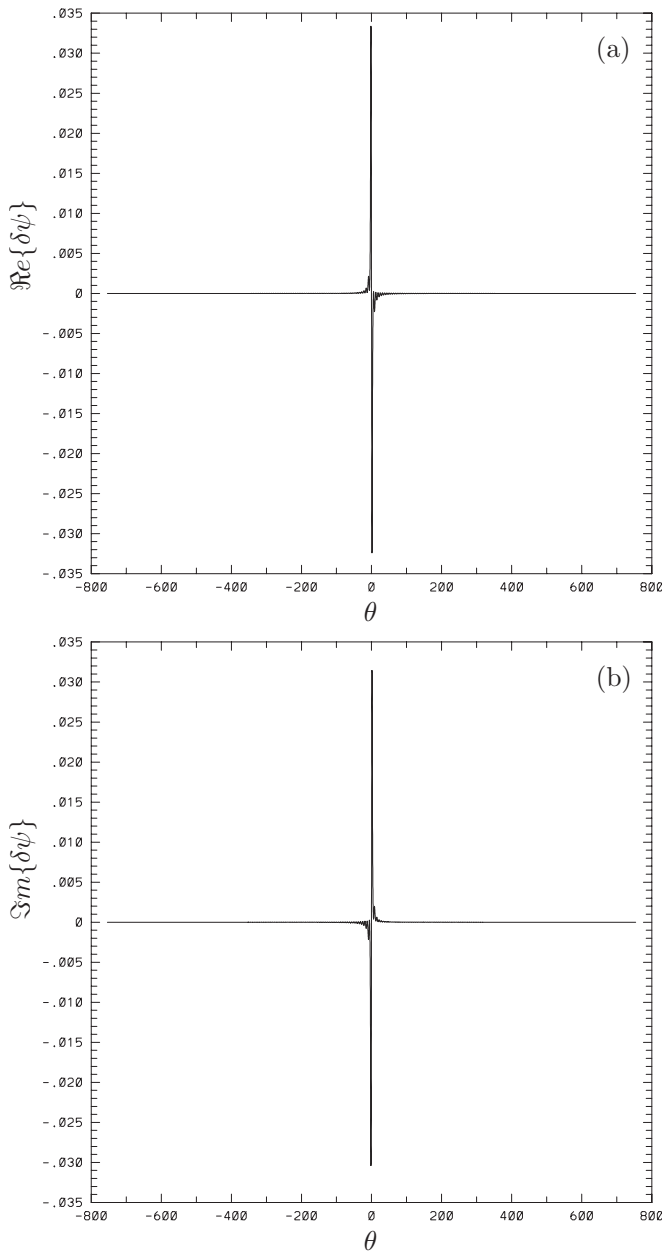
FIG. 9. Real and imaginary parts of the perturbed radial magnetic field for CITM.



FIG. 10. Real and imaginary parts of the CITM eigenfunction in configuration space.

$\bar{\Sigma}'$ in Sec. II B 1. We use a conserve estimate $\Sigma'^* = 10^{-5}$. The real and imaginary parts of the eigenfunction $\delta\varphi$ are given in Fig. 8, while the real and imaginary parts of the perturbed radial magnetic field $\delta\psi$ are plotted in Fig. 9. Figures 10 and 11 give, respectively, $\delta\varphi$ and $\delta\psi$ plots in the configuration space. The growth rate for this case is $\gamma_N = 4.2 \times 10^{-3}$. From Figs. 8–11, one can see that both $\delta\varphi$ and $\delta\psi$ become complex and nonsymmetric for $\delta\varphi$ and nonantisymmetric for $\delta\psi$. The tearing-parity of the modes appears as one can expect. The perturbed radial magnetic field $\delta\psi$ becomes finite at the singular layer. For real part $\Re e\{\delta\psi\}_{\hat{x}=0} = 2.2 \times 10^{-3}$, the imaginary part $\Im m\{\delta\psi\}_{\hat{x}=0} = 2.4 \times 10^{-3}$. When $\Sigma'^*$ or $\alpha$ increases, the strength of perturbed radial magnetic field at the rational surface becomes even bigger. Noting that $\Delta' = 0$ in this $s-\alpha$ equilibrium model, the classical tearing modes are
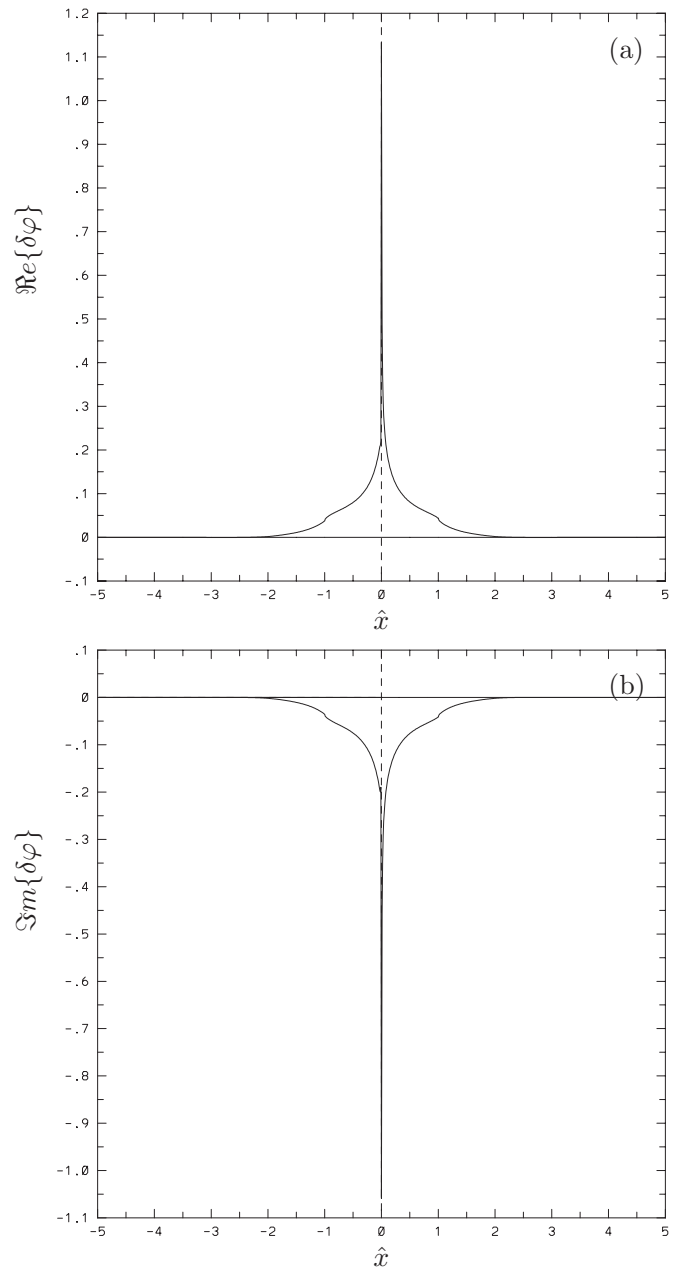
nonexistant in this case. A finite perturbed radial magnetic field $\delta\psi$ at the rational surface represents a conversion from restive ballooning modes given in Figs. 4–7 to CITMs in Figs. 8–11.

## C. Nonlinear analysis

Next, we analyze this mode conversion process nonlinearly. We employ the conventional approach based on the Rutherford equation[19] to show how a current sheet results as pressure-driven instabilities develop. For simplicity we use cylindrical geometry $(r, \theta, \phi)$, where $r$ is the minor radius of the tokamak and $\phi$ is the toroidal angle. As usual, the singular layer at the rational surface and the outer regions are analyzed separately. In the outer regions, the resistive effect
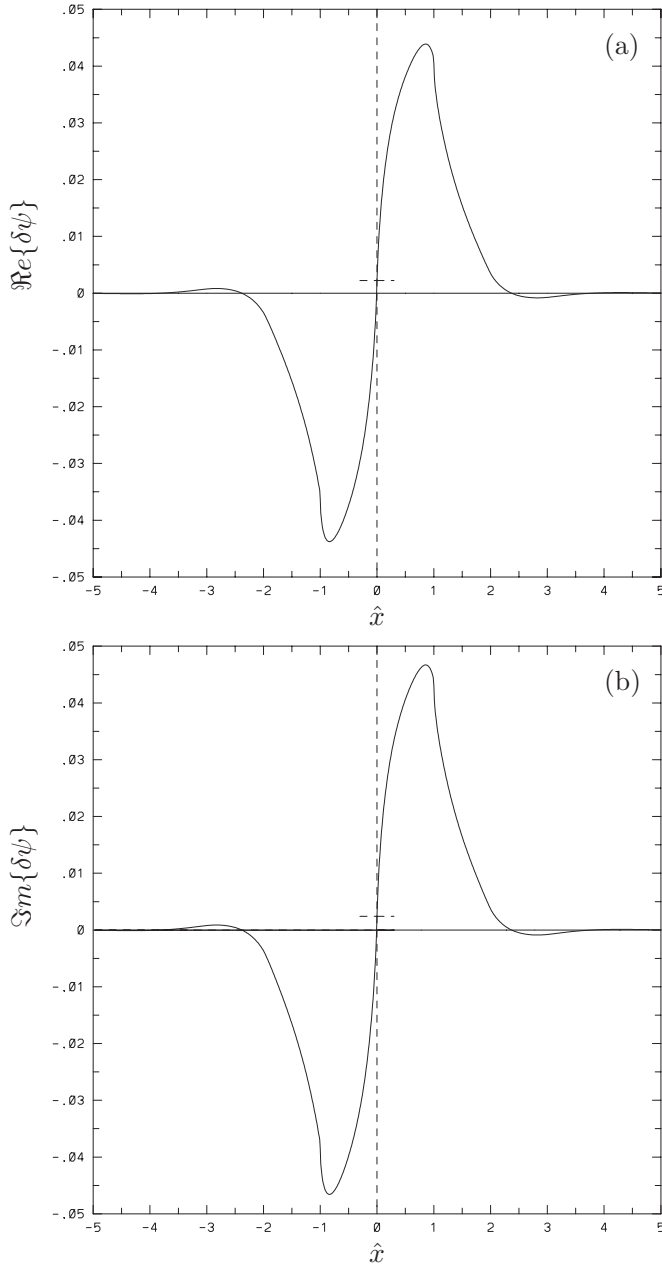
FIG. 11. Real and imaginary parts of the perturbed radial magnetic field for CITM in configuration space.



FIG. 12. (Color online) Linear eigenfunctions for the cases with (solid) and without (dashed) resistivity gradient effect.

is usually negligible and ideal MHD theory applies. Therefore, we focus our investigations on the singular layer.

The equations for the tearing mode and for the pressure-driven mode govern the singular layer.[20] With the resistivity gradient effect taken into account and the perturbation of resistivity assumed to result only from convection as in Ref. 9, these equations can be written as

$$\frac{\partial^2 \delta B_r}{\partial x^2} = \tau_r \frac{\partial \delta B_r}{\partial t} + i\frac{n\tau_r B s}{R} x \frac{\partial \xi_r}{\partial t} + i\frac{m\tau_r J_\phi}{\sigma r_s^2} \frac{d\ln\sigma}{dx} \xi_r, \quad (16)$$

$$i\frac{R}{nB_\phi} s x \frac{d^2 \delta B_r}{dx^2} + \frac{\gamma^2}{n^2 \omega_A^2} \frac{d^2 \xi_r}{dx^2} - \left(\frac{1}{4} - D\right) \xi_r = 0, \quad (17)$$

where $\delta B_r$ is the perturbed radial magnetic field, $\tau_r = \sigma r_s^2$ is the resistive time, $r_s$ is the minor radius at the rational sur-

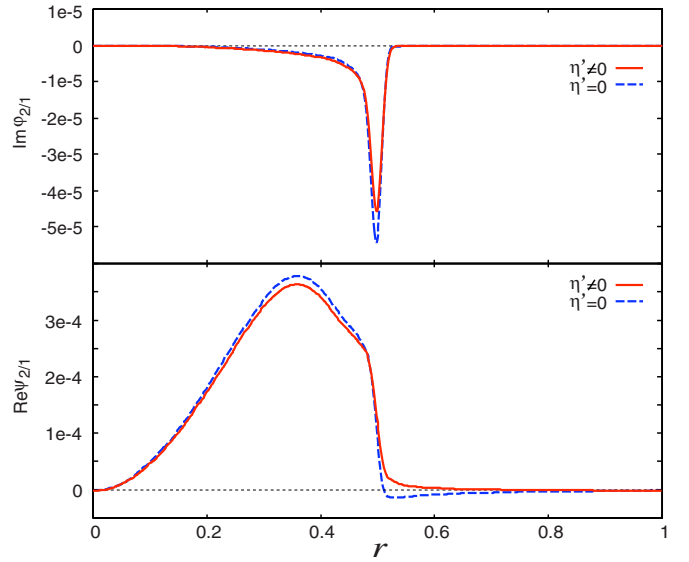face, $R$ is the major radius, and $D$ is the so-called Mercier index. Equations (16) and (17) correspond to Eqs. (9) and (8) in the ballooning mode representation space.

Equations (16) and (17) constitute a complete set of equations describing the behavior of the singular layer. These equations have two types of solutions: tearing-type modes, which have even parity for $\delta B_r$ at the rational surface, and pressure-driven modes, which have odd parity.[20] Here we consider the even parity (i.e., tearing) modes. The last two terms in Eq. (16) represent the coupling of pressure-driven modes. As shown in Ref. 19, the second term on the right-hand side of Eq. (16) can be removed by a suitable surface average. Then, following the procedure used to derive the classical Rutherford equation in Ref. 19, one can extend the linear tearing mode Eq. (16) into the nonlinear version:

$$\tau_r \frac{\partial w}{\partial t} = \frac{\sqrt{Rr_s}}{\sqrt{2A}}\Delta' + \hat{\Sigma}' \sqrt{Rr_s}\frac{\xi_r(r_s)}{w}, \quad (18)$$

where $w = 4\sqrt{(Rr_s/ns)(\delta B_r/B)}$ is the width of the magnetic island, $\Delta' = (d\delta B_r/dx)/\delta B_r|_{r_s^-}^{r_s^+}$, $\hat{\Sigma}' = (8qJ_\phi/B_\phi s^{3/2}\sigma)|d\ln\sigma/dr|\tau_r$ describes the coupling of pressure-driven modes, and $A \approx 0.7$ as given in Ref. 19. We estimate the magnitude of $\hat{\Sigma}'$. Similar to the estimate of $\Sigma'^*$ for ballooning mode in Sec. II B 2, the dimensionless parameter $\hat{\Sigma}'/\tau_r$ is of order of a hertz. In driving Eq. (18), we have not included NTM effects, such as the bootstrap current,[1,2] the polarization current,[21] and the transport-induced current.[22] In our theory, the current sheet is related to the equilibrium Ohmic current and is due to the convection of equilibrium current by unstable pressure-driven modes. Therefore, the second term on the right-hand side of Eq. (18) represents an additional driving mechanism for tearing modes. Note that in the derivation of the modified Rutherford Eq. (18), the "O" point of the magnetic island is located where the perturbed electric conductivity is minimum, which is consistent with the physics analysis described in Sec. II A.

From Eq. (18) one can derive a new stability criterion for tearing modes

$$\Delta' + \hat{\Sigma}' \sqrt{2} A \frac{\xi_r(r_s)}{w} < 0. \tag{19}$$

This new criterion differs from the classical tearing mode stability criterion $\Delta' < 0$ by having an additional driving term. We note that $\xi_r(r_s)$ in Eq. (19) needs to be determined by the vorticity equation. The key point is that $\xi_r$ contains generally even parity part and therefore is finite at the rational surface (see, for instance, Ref. 17 or Fig. 12). This can also be explained by the simplified ideal MHD, zero beta singular layer equation: $d/dx(x^2 + \gamma^2)d\xi_r/dx = 0$. The solution of this equation is simply $\xi_r = c_1 \text{arctg}(x/\gamma) + c_0$, where $c_{1,0}$ are constants. Here $\xi(r_s) = c_2$ represents the finite even parity part. As the pressure-driven modes grow, the second term in Eq. (19) can override the first term, so that CITMs are excited and magnetic islands formed. The second term in Eq. (19) is inversely proportional to the island width. This indicates that this term can play a role in the early developing stage of pressure-driven modes. As in the theory for NTMs, one can anticipate that the strict singularity in $w$ can be removed by taking into account finite Larmor radius effects.

We can discuss the order of nonlinear development. Dropping the first term on the right, Eq. (18) gives $w^2/\xi_r\sqrt{Rr_s} \sim \hat{\Sigma}'/\gamma\tau_r$. As discussed earlier, we can order $\hat{\Sigma}'/\tau_r$ to a hertz. Using ion Larmor radius to estimate $w$, the ratio $w/\sqrt{Rr_s}$ is about $10^{-3}$. Therefore, for $\gamma \lesssim 10^3$ Hz, one has $w/\xi_r \gtrsim 1$. This is especially true for marginally unstable modes. Note further that $w$ and $\xi_r$ have the same dimension and plasma response to island width $w$ is quick due to the parallel mobility. Therefore, one can anticipate that the local pressure profile flattening due to the formation of magnetic islands can occur immediately after the marginal stability and before the interchange-type modes saturated. Certainly, there may exist another scenario, in which the plasma runs very quickly over the marginal instability, so that the interchange-type modes get saturated first.[23]

In above analysis, we have considered electromagnetic perturbations. Actually, electrostatic modes can have the same type of effect on tearing modes. For electrostatic modes, the radial displacement $\xi_r$ in the second term of Eq. (18) is related to the electrostatic perturbation $\delta\phi$ as follows: $\xi_r \propto \nabla r \cdot \mathbf{B} \times \nabla \delta\phi / \gamma B^2$. Consequently, the electrostatic quasineutrality condition can be used to replace the pressure-driven mode Eq. (17). Hence, unstable electrostatic modes (e.g., drift waves) can also convert to CITMs.

Now we exhibit a numerical example for this new mode conversion. Since CITMs belong to nonclassical tearing modes, we will consider the NTM-like scenario in which classical tearing modes are stable. There are many types of such scenarios in the finite beta confinement. Here, we use a reduced MHD model in cylindrical geometry to simulate a NTM-like scenario. This model has to do with confinement at finite beta. Resistivity is small for finite beta. Classical g-modes of the tearing mode type are highly localized when the resistivity is small, and viscosity (or finite Larmor radius) effects can suppress these localized modes. Hence, fairly large interchange-type modes are prevalent, due to the finite beta drive. The basic set of linear equations is as follows:

$$\frac{\partial \delta U}{\partial t} = [\psi, J]_1 - \frac{\partial \delta J}{\partial z} + \kappa_{r0} \frac{1}{r} \frac{\partial \delta p}{\partial \theta} + \nu \nabla_\perp^2 \delta U,$$

$$\frac{\partial \delta \psi}{\partial t} = [\psi, \varphi]_1 - \frac{\partial \delta \varphi}{\partial z} + \eta \nabla_\perp^2 \delta \psi + \eta \frac{d \ln \eta/dr}{d \ln \beta/dr} \delta p,$$

$$\frac{\partial \delta p}{\partial t} = [p, \varphi]_1 + \frac{1}{r} \frac{\partial \beta}{\partial r} \frac{\partial \delta \varphi}{\partial \theta} + \chi \nabla_\perp^2 \delta p,$$

where $-i\omega\boldsymbol{\xi} = \mathbf{z} \times \nabla \delta\varphi$, $\delta\mathbf{B} = \nabla \delta\psi \times \mathbf{z}$, $\delta U = \nabla_\perp^2 \delta\varphi$, $\delta J = \nabla_\perp^2 \delta\psi$, $[a,b]_1 = [(\partial a/\partial r)(\partial \delta b/\partial \theta) - (\partial b/\partial r)(\partial \delta a/\partial \theta)]/r$, $z = R\phi$, $R/a = 10$, $\varphi = 0$. Also, we model the safety factor profile as $q(r) = q_a/(2 - r^2) + \beta_q(r - r_s) \exp\{-(r - r_s)^2/L_q^2\}$, with $q_a = 3.5$, $\beta_q = -0.3$, $L_q = 0.1$, and $r_s = 0.5$; we take the profile for the ratio between plasma energy and magnetic energy to be $\beta(r) = (\beta_0 - \beta_1)(1 - r^2) + \beta_1$, with $\beta_0 = 0.01$ and $\beta_1 = 0.001$, $\kappa_{r0} = -B_\theta^2/r$; and we assume $10^{-8}$ as the value for the resistivity $\eta$, viscosity $\nu$, and thermal conductivity $\chi$. We examine the case of the $n = 1$, $m = 2$ interchange-type mode as an example. For such small resistivity, the tearing-type classical g-mode is highly localized and therefore suppressed by viscosity (or finite Larmor radius) effects.

In our numerical scheme, Fourier decomposition is used in poloidal and toroidal directions, and finite difference method is used in the radial direction. The LAPACK library is used in calculating eigenvalues of the corresponding matrix. The code is benchmarked against the asymptotic matching method successfully at small resistivity regime (for the case without resistivity gradient effect). The radial grid number is 200 with grid accumulation around the rational surface. This is sufficient for this type of calculation.

Figure 2 shows the linear eigenmode as a function of minor radius for cases with (solid curve) and without (dashed curve) resistivity gradient effect. With no resistivity gradient effect taken into account, the mode is a pure resistive interchange mode (with computed $\Delta' = -4.15$), for which the radial magnetic perturbation $\psi$ at the rational surface is negligible. The linear growth rate normalized to the Alfvén frequency is $3.2 \times 10^{-5}$. When the resistivity gradient effect is taken into account, however, the radial magnetic perturbation $\psi$ at the rational surface becomes finite. Consequently, a mode of tearing parity appears, with growth rate $4.1 \times 10^{-5}$. This confirms the conversion of pressure-driven modes to CITMs. Then, since a finite radial magnetic perturbation exists at the rational surface, a magnetic island is formed. Due to the large parallel thermal conductivity, the pressure profile is flattened at the rational surface over the width of the magnetic island. As discussed in the last paragraph, we can focus on the nonlinearity of the island-induced pressure profile flattening.

We adopt this simplified pressure profile evolution to perform a quasilinear analysis of the CITMs, as is done for NTMs. Figure 3 shows the quasilinear evolution of the radial magnetic field (or equivalently, the island width $w$) and the quasilinear growth rate. The numerical results in Fig. 13 indicate that the width of the magnetic island increases in time.
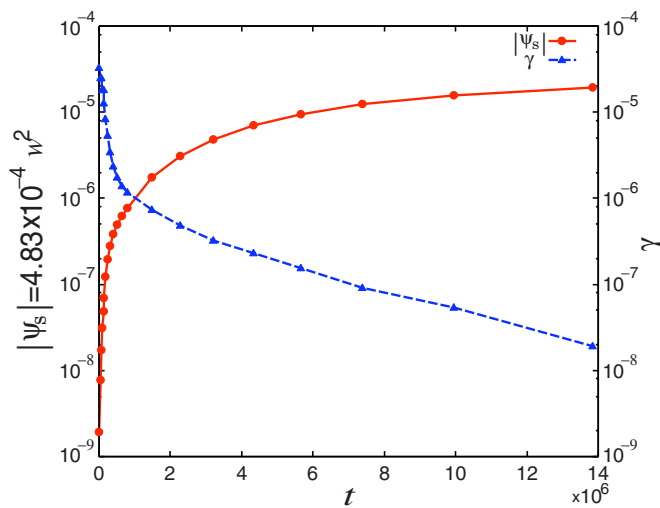
FIG. 13. (Color online) Quasilinear evolution of the radial magnetic field $\psi$ (or the island width, solid curve) and quasilinear growth rate (dashed) with time (normalized by $a/V_A$). The half island width evolves from 0.001 to 0.1.



FIG. 14. The schematic picture for $q$ profile (solid curve) and the directions of island rotation transforms at three different radii (dashed curves) in the reversed shear configuration.

Since the pressure profile flattening width increases with the island width, the quasilinear growth rate gradually decreases. Eventually, the island width saturates.

## III. DISCUSSION

In this section, we discuss the CITM effect on anomalous transport and MHD phenomena. Note that the interchange mode is fundamental to the magnetically confined plasmas. Note also that tokamak carries the toroidal current and that there generally exists current gradient in tokamak confinement. The mode conversion from interchange to tearing types of modes in tokamaks, i.e., the existence of CITMs, can affect on anomalous transport and MHD phenomena.

We first discuss anomalous transport in tokamaks. There are two types of anomalous transport theories in this field: the conventional one that is based on the turbulent eddies through nonlinear coupling and the field line stochasticity one that is based on destroyed magnetic surfaces.[6,24,25] Both theories explain the nonclassical radial transport step size. In the conventional theory, the turbulent eddies characterize the step size. In the theory based on the destroyed magnetic surfaces the step size is characterized by the magnetic island width and nearby islands (or their stochastic field lines) reconnection. The importance aspect of the theory based on the destroyed magnetic surfaces is that it can naturally explain the source of electron transport.[6] Since electrons have large parallel thermal velocity, their transport can be dramatically enhanced by the broken magnetic surfaces. The question is what causes the magnetic surfaces to brake in a axisymmetric tokamak. The microtearing mode theories have been proposed in this field, for example, that based on the electron temperature gradient modes.[7] In these theories, the field line reconnection (or the formation of islands) results from the turbulence-induced anomalous current sheet. In our current CITM theory, we show that the current sheet can occur at the first place, as soon as the existing current-gradient in tokamak is taken into account. Since interchange-type of modes are universal, the formation of the magnetic islands in a to-
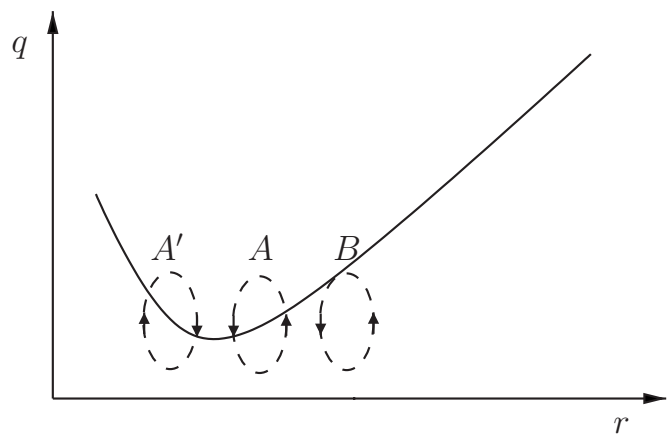
kamak which is unstable to interchange type of modes can be general. This is just like what we have examined for interchange/ballooning modes in Sec. II. Note that the conventional transport theories rely on the nonlinear development of the interchange type of modes. Our CITM theory shows that the underlying instabilities for conventional transport theories can converted to CITMs and cause the formation of the magnetic islands. This leads to the anomalous transport described by the theories based on the destroyed magnetic surfaces.[6,25] Due to this critical change, we further discuss some concerned issues for anomalous transport.

First, we discuss the transport barrier phenomenon. The reduced particle transport at the reversed shear region has been reported in the simulations based on the theories of broken magnetic surfaces.[24,25] The conversion from the interchange-type of modes to CITMs gives a support to the transport barrier theory based on the broken magnetic surfaces. An intuitive picture for transport barrier is given as follows. As shown in Fig. 14, the island (including the associated stochastic field) rotational transform reverses direction across a $q$ minimum. As islands grow and reconnect in the case without magnetic shear reversal (islands $A$ and $B$ and their associated stochastic field), magnetic energy can be released and the radial transport step size increased. However, this type of island-island reconnection is prohibited at the stationary surface of safety factor in the case of reversed shear (islands $A$ and $A'$ and their associated stochastic field). Enhanced transport due to island-island and their associated stochastic field reconnection in the normal shear case has been reported in the reversed field pinch experiments.[26] The reconnection forbidden layers are observed at the $q$ maximum in the reversed field pinch experiments.[27] These layers are termed as the so-called ghost surfaces. Ghost surfaces were originally introduced for the standard map to denote surfaces which are nonintersecting (in this context, they are called ghost circles).[28,29] We point out here that at $q$ stationary surface such type of ghost surfaces can be formed naturally due to different wiring directions of island (and their associated stochastic region) field lines on the opposite sides of $q$ stationary surface.

The other important issue is the formation of blob filamentary (or intermittent) structures, as observed experimentally.[30–35] Magnetic islands and blob filaments have similar spatial structure. Both are mainly aligned along the magnetic filed lines, are characterized by local poloidal homogeneity around the filament axis, and have saturated size. Experimental observations show that the blobs at the plasma edge are brighter than the surrounding area, no matter on which sides: toward core plasma or toward vacuum region.[35] From Fig. 1, one can see that islands formed by the magnetic islands bring cold and hot plasmas together. Therefore, one can anticipate that charge-recombination process occurs at the island regions. This makes blobs brighter. Actually, many numerical simulations of blob phenomenon relies on resistive MHD for formation of the magnetic islands.[36] Our theory indicates that CITMs can be a candidate for explanation the formation of this type of islands.

The field line stochasticity-induced transport picture is also consistent with the formation of H-mode confinement in tokamak experiments.[37] First, we note that the rotation curvature can prevent island reconnection, in the same topologic consideration as that proposed for suppressing turbulence eddies.[38] Second, we note that H-mode with negative charge at the plasma edge usually has better particle confinement property than that with positive edge charge.[23] Note that the stochasticity-induced transport is characterized by the parallel motion of the particles. Since electrons have large parallel velocities, they can then play a key role in transport. Therefore, one can expect that negative charges at the plasma edge can help to reduce the core electron transport. Our theory can give a possible candidate for island formation for stochasticity-induced transport given in Ref. 6.

Furthermore, as shown in Sec. II, the conversion to CITMs occurs immediately after the marginal stability limit. This may explain why many linear marginal stability criteria—for example, those for peeling-ballooning modes[39,40]—remain relevant for explaining the experimental observations.

Besides anomalous transport, CITMs can also help to explain MHD phenomena observed in tokamak experiments. For example, the current CITM picture can provide a natural explanation of the conversion from $n=1$ internal kink modes to tearing modes for explaining the tokamak plasma internal disruptions.[4,5] Note that CITMs is a new type of nonclassical tearing modes and experimentally observed NTMs usually occur at high beta confinement.[3] At high beta, interchange-type of modes are likely to develop. Our theory may explain why sometimes the resistive wall modes and NTMs are tied together in the experimental observations.

## IV. SUMMARY

In summary, we have shown that another type of nonclassical tearing mode exists in tokamaks: viz., called CITMs. We explained the physics underlying these modes and demonstrated their existence both analytically with the modified Rutherford equation and also numerically with a reduced MHD code. Our results indicate that systems that are unstable to pressure-driven modes of interchange type are prone to become unstable also to current-driven tearing modes. We have explained how the excitation of the new CITMs allows another path for the development of anomalous transport in tokamaks. These new modes could provide natural explanations for many anomalous transport features, such as the nonclassical transport step size, especially for electron transport, the observation of filamentary (or intermittent) structures, the formation of internal transport barriers, the H-mode confinement, etc. The CITMs may also help to understand certain MHD phenomena, such as the coexistence of kink and tearing modes and the internal disruption.

In this paper, we have discussed many experimental phenomena. They are complex in nature. One can expect that further theoretical and experimental efforts are required to fully clarify them. Nevertheless, with so many coincidences between our current theory and experimental observations we believe that the conversion from interchange-type of modes to tearing modes is an important physics phenomenon in tokamaks. It deserves to be further investigated in the future.

[1]R. Carrera, R. D. Hazeltine, and M. Koschenreuther, Phys. Fluids **29**, 899 (1986).
[2]J. D. Callen, W. X. Qu, K. D. Siebert, B. A. Carreras, K. C. Shang, and D. A. Spong, *Plasma Physics and Controlled Nuclear Fusion Research* (International Atomic Energy Agency, Vienna, 1987), Vol. 2, p. 157.
[3]R. J. La Haye, Phys. Plasmas **13**, 055501 (2006).
[4]J. Wesson, *Tokamaks* (Cambridge University Press, Oxford, 2004).
[5]B. B. Kadomtsev, Sov. J. Plasma Phys. **1**, 389 (1975).
[6]A. B. Rechester and M. N. Rosenbluth, Phys. Rev. Lett. **40**, 38 (1978).
[7]J. W. Connor, S. C. Cowley, and R. J. Hastie, Plasma Phys. Controlled Fusion **32**, 799 (1990).
[8]P. Zhu, C. R. Sovinec, and C. C. Hegna, Bull. Am. Phys. Soc. **51**, 38 (2006).
[9]H. P. Furth, J. Killeen, and M. N. Rosenbluth, Phys. Fluids **6**, 4826 (1963).
[10]R. J. Hastie, F. Militello, and F. Porcelli, Phys. Rev. Lett. **95**, 065001 (2005).
[11]D. Correa-Restrepo, Z. Naturforsch. C **37a**, 848 (1982).
[12]J. W. Van Dam and Y. C. Lee, *Proc. of the Advanced Bumpy Torus Concept Workshop* (Oak Ridge, Tennessee, 1980), p. 471.
[13]J. W. Connor, R. J. Hastie, and J. B. Taylor, Phys. Rev. Lett. **40**, 396 (1978).
[14]J. L. Johnson and J. M. Greene, Plasma Phys. **9**, 611 (1967).
[15]M. Abramowitz and I. A. Stegun, *Handbook of Mathematical Functions* (Dover, New York, 1972), p. 503.
[16]B. R. Suydam, Proceedings of the Second UN international Conference PUAE, United Nations, Geneva, 1958, Vol. 31, p. 157.
[17]L.-J. Zheng and M. Kotschenreuther, J. Comput. Phys. **211**, 748 (2006).
[18]J. Nührenberg and R. Zille, Phys. Lett. A **129**, 113 (1988).
[19]P. H. Rutherford, Phys. Fluids **16**, 1903 (1973).
[20]A. H. Glasser, J. M. Greene, and J. L. Johnson, Phys. Fluids **18**, 875 (1975).
[21]F. L. Waelbroeck, J. W. Connor, and H. R. Wilson, Phys. Rev. Lett. **87**, 215003 (2001).
[22]R. Fitzpatrick, Phys. Plasmas **2**, 825 (1995).
[23]R. R. Weynants, G. van Oost, G. Bertschinger, J. Boedo, P. Brys, T. Delvigne, K. H. Dippel, F. Durodie, H. Euringer, K. H. Finken, D. S.

Gray, J. D. Hey, D. L. Hillis, J. T. Hogan, L. Konen, R. Leners, A. M. Messiaen, A. Pospieszczyck, U. Samm, R. P. Schorn, B. Schweer, G. Telesca, R. van Nieuwenhove, and P. E. Vandenplas, Nucl. Fusion **32**, 837 (1992).

[24]D. del-Castillo-Negrete and P. J. Morrison, Phys. Fluids **A5**, 948 (1993).

[25]P. J. Morrison and A. Wurm, Scholarpedia J. **4**, 3551 (2009).

[26]J. S. Sarff, Bull. Am. Phys. Soc. **54**, 178 (2009).

[27]M. E. Puiatti, A. Alfier, F. Auriemma, S. Cappello, L. Carraro, R. Cavazzana, S. Dal Bello, A. Fassina, D. F. Escande, P. Franz, M. Gobbin, P. Innocente, R. Lorenzini, L. Marrelli, P. Martin, P. Piovesan, I. Predebon, F. Sattin, G. Spizzo, D. Terranova, M. Valisa, B. Zaniol, L. Zanotto, M. Zuin, M. Agostini, V. Antoni, L. Apolloni, M. Baruzzo, T. Bolzonella, D. Bonfiglio, F. Bonomo, A. Boozer, M. Brombin, A. Canton, R. Delogu, G. De Masi, E. Gaio, E. Gazza, L. Giudicotti, L. Grando, S. C. Guo, G. Manduchi, G. Marchiori, E. Martines, S. Martini, S. Menmuir, B. Momo, M. Moresco, S. Munaretto, L. Novello, R. Paccagnella, R. Pasqualotto, R. Piovan, L. Piron, A. Pizzimenti, N. Pomphrey, P. Scarin, G. Serianni, E. Spada, A. Soppelsa, S. Spagnolo, M. Spolaore, C. Taliercio, N. Vianello, A. Zamengo, and P. Zanca, Plasma Phys. Controlled Fusion **51**, 124031 (2009).

[28]C. Golé, J. Differ. Equ. **97**, 140 (1992).

[29]R. S. MacKay and M. R. Muldoon, Phys. Lett. A **178**, 245 (1993).

[30]D. H. J. Goodall, J. Nucl. Mater. **111–112**, 11 (1982).

[31]S. J. Zweben, Phys. Fluids **28**, 974 (1985).

[32]J. I. Boedo, D. Rudakov, R. Moyer, S. Krasheninnikov, D. Whyte, G. McKee, G. Tynan, M. Schaffer, P. Stangeby, P. West, S. Allen, T. Evans, R. Fonck, E. Hollmann, A. Leonard, A. Mahdavi, G. Porter, M. Tillack, and G. Antar, Phys. Plasmas **8**, 4826 (2001).

[33]J. L. Terry, R. Maqueda, C. S. Pitcher, S. J. Zweben, B. LaBombard, E. S. Marmar, A. Y. Pigarov, and G. Wurden, J. Nucl. Mater. **290–293**, 757 (2001).

[34]D. L. Rudakov, J. A. Boedo, R. A. Moyer, S. Krasheninnikov, A. W. Leonard, M. A. Mahdavi, G. R. McKee, G. D. Porter, P. C. Stangeby, J. G. Watkins, W. P. West, D. G. Whyte, and G. Antar, Plasma Phys. Controlled Fusion **44**, 717 (2002).

[35]A. Kirk, N. B. Ayed, G. Counsell, B. Dudson, T. Eich, A. Herrmann, B. Koch, R. Martin, A. Meakins, S. Saarelma, R. Scannell, S. Tallents, M. Walsh, H. R. Wilson, and MAST Team, Plasma Phys. Controlled Fusion **48** B433 (2006).

[36]D. Reiser, Phys. Plasmas **14**, 082314 (2007).

[37]F. Wagner, G. Becker, K. Behringer, D. Campbell, A. Eberhagen, W. Engelhardt, G. Fussmann, O. Gehre, J. Gernhardt, G. V. Gierke, G. Haas, M. Huang, F. Karger, M. Keilhacker, O. Klüber, M. Kornherr, K. Lackner, G. Lisitano, G. G. Lister, H. M. Mayer, D. Meisel, E. R. Müller, H. Murmann, H. Niedermeyer, W. Poschenrieder, H. Rapp, H. Röhr, F. Schneider, G. Siller, E. Speth, A. Stäbler, K. H. Steuer, G. Venus, O. Vollmer, and Z. Yü, Phys. Rev. Lett. **49**, 1408 (1982).

[38]L. J. Zheng and M. Tessarotto, private communication (1997).

[39]J. W. Connor, Plasma Phys. Controlled Fusion **40**, 531 (1998).

[40]P. B. Snyder, H. R. Wilson, and X. Q. Xu, Phys. Plasmas **12**, 056115 (2005).